Earth's Future

RESEARCH ARTICLE
10.1029/2018EF001020

Projections of Human Exposure to Dangerous Heat in African Cities Under Multiple Socioeconomic and Climate Scenarios

Guillaume Rohat[1,2,3], Johannes Flacke[2], Alessandro Dosio[4], Hy Dao[1,5], and Martin van Maarseveen[2]

[1]Institute for Environmental Sciences, University of Geneva, Geneva, Switzerland, [2]Faculty of Geo-Information Science and Earth Observation, University of Twente, Enschede, The Netherlands, [3]National Center for Atmospheric Research (NCAR), Boulder, CO, USA, [4]European Commission, Joint Research Centre, Ispra, Italy, [5]United Nations Environment Programme DEWA/GRID, Geneva, Switzerland

Key Points:
- Exposure to dangerous heat in African cities will increase by a multiple of 20–52 to reach 86–217 billion person-days per year by the 2090s
- Future exposure is predominantly driven by changes in urban population alone or by concurrent changes in climate and urban population
- Shifting from a high to a low urban population growth pathway reduces exposure by as much as a shift from a high to a low emissions pathway

Supporting Information:
- Supporting Information S1
- Table S1
- Data Set S1

Correspondence to:
G. Rohat,
guillaume.rohat@unige.ch

Citation:
Rohat, G., Flacke, J., Dosio, A., Dao, H., & van Maarseveen, M. (2019). Projections of human exposure to dangerous heat in African cities under multiple socioeconomic and climate scenarios. *Earth's Future*, *7*. https://doi.org/10.1029/2018EF001020

Received 21 AUG 2018
Accepted 2 APR 2019
Accepted article online 4 APR 2019

Abstract Human exposure to dangerous heat, driven by climatic and demographic changes, is increasing worldwide. Being located in hot regions and showing high rates of urban population growth, African cities appear particularly likely to face significantly increased exposure to dangerous heat in the coming decades. We combined projections of urban population under five socioeconomic scenarios—shared socioeconomic pathways—with projections of apparent temperature under three representative concentration pathways in order to explore future exposure to dangerous heat across 173 large African cities. Employing multiple shared socioeconomic pathway and representative concentration pathway combinations, we demonstrated that the aggregate exposure in African cities will increase by a multiple of 20–52, reaching 86–217 billion person-days per year by the 2090s, depending on the scenario. The most exposed cities are located in Western and Central Africa, although several Eastern African cities showed an increase of more than 2,000 times the current level by the 2090s, due to the emergence of dangerous heat conditions combined with steady urban population growth. In most cases, we found future exposure to be predominantly driven by changes in population alone or by concurrent changes in climate and population, with the influence of changes in climate alone being minimal. We also demonstrated that shifting from a high to a low urban population growth pathway leads to a slightly greater reduction in aggregate exposure than shifting from a high to a low emissions pathway (51% vs. 48%). This emphasizes the critical role that socioeconomic development plays in shaping heat-related health challenges in African cities.

Plain Language Summary Very hot and humid weather often leads to numerous health issues, ranging from heat cramps to death. Due to changing climatic conditions and to demographic growth, the number of people exposed to very hot and humid days is increasing worldwide. This is particularly the case across the African continent, where population growth is rapidly increasing and very hot and humid days are becoming more and more frequent, particularly in tropical areas. In this study, we consider more than 150 large African cities across 43 countries and project the number of people that will be exposed to dangerous heat conditions. Our projections suggest that this number will be 20 to 52 times higher at the end of the 21st century than currently. Large cities in Western and Central Africa appear to be particularly at risk, whereas cities in Southern Africa will remain relatively unscathed. We also show that a restrained urban demographic growth could lead to a 50% reduction in the number of people exposed to dangerous heat conditions. Population and urbanization policies should be part of the wide range of urban climate adaptation options in order to minimize future exposure to extreme heat.

1. Introduction

As recently highlighted in the 2018 Revision of World Urbanization Prospects (WUP; United Nations, 2018), African cities are currently experiencing unprecedented growth, driven by factors ranging from technology-driven development to environmental changes affecting primary rural production (Lwasa et al., 2018). Leading the global urbanization trend, the African urban population is expected to at least triple in the 40-year period from 2010 to 2050, reaching 21% of the future world's urban population. Global warming—

even if limited to +1.5 °C—will pose serious threats to many urban populations in Africa (Pelling et al., 2018). The effects of climate change on African cities include climate-induced droughts, water scarcity, coastal flooding, salt-water intrusion, river floods, desertification, and heat waves (Lwasa et al., 2018). The frequency, duration, and intensity of the latter are expected to increase considerably in the 21st century over the African continent, particularly in subtropical areas (Dosio, 2017; Dosio et al., 2018; Russo et al., 2016). Such an increase has significant implications for human health, as extreme temperatures are strongly linked to heat stroke and mortality (Gasparrini, Guo, Hashizume, Kinney, et al., 2015; Gasparrini, Guo, Hashizume, Lavigne, et al., 2015; Mora et al., 2017).

Driven by both high population growth and significant changes in climatic conditions, future exposure to dangerous heat in Africa is projected to show the highest increase worldwide during the 21st century, with South Asia being close behind (Coffel et al., 2018; Dong et al., 2015; Jones et al., 2018; Liu et al., 2017; Matthews et al., 2017). Recent regional studies conducted in Eastern Africa (Harrington & Otto, 2018) and across the Great African Lakes region (Asefi-Najafabady et al., 2018) have provided a closer look at the effects of changes in socioeconomic and climatic conditions on future exposure to dangerous heat in some parts of Africa. However, the effects of such factors on the urban populations of the many large African cities remain to be explored. Such a lack of focus on African cities may be attributable to the absence of population projections at the city scale, under different socioeconomic scenarios. In this study, we use both nonspatial (NS) and spatial (SP) methods to provide urban population projections for African cities under several socioeconomic scenarios, namely, the shared socioeconomic pathways (SSPs; O'Neill et al., 2017). These projections are then combined with projections of extreme temperature under different levels of climate forcing, namely, the representative concentration pathways (RCPs; van Vuuren et al., 2011), in order to assess future human exposure to dangerous heat in African cities under different combinations of socioeconomic and climate scenarios.

Additionally, we noted that existing studies fell short in exploring uncertainties due to various levels of socioeconomic development, as they generally considered only two different SSPs (out of the five) and employed no more than four different combinations of RCPs and SSPs, whereas many more combinations are likely to occur (Kriegler et al., 2012). In this study, besides shedding light on a new and critical case study (viz., the African cities), we also complement the existing literature by exploring the full range of uncertainties linked to the various societal pathways—that is, employing the five SSPs—and to their multiple plausible combinations with three levels of radiative forcing (RCPs). Finally, most of the existing studies—irrespective of the spatial coverage and the scenarios—found that demographic change has a significant influence on future exposure to dangerous heat, although more often than not lesser than that of climate change (e.g., Asefi-Najafabady et al., 2018). Because African cities will likely experience the highest levels of urban population growth worldwide (United Nations, 2018), the influence of demographic change on future exposure to extreme heat is likely to be substantial and may even be greater than the effect of climate change alone. In this paper, we test this assumption by (i) thoroughly disentangling the individual contributions of changes in climatic and socioeconomic conditions and (ii) assessing the extent to which exposure could be limited by shifts in socioeconomic and climatic pathways.

2. Methods

2.1. Selection of Sample Cities

In this study we focus on large African cities that are listed in the 2014 Revision of WUP (United Nations, 2014)—the 2018 Revision of WUP being unavailable when cities were selected—that is, cities that have a total population exceeding 300,000 inhabitants for the year 2014. This yields a sample of 185 cities, with population size ranging from 300,000 to 18 million (M) inhabitants (Table S1 in the supporting information). Due to the merging of several contiguous cities (see section 2.2 and Table S2), the initial sample was reduced to 173 different cities. These are located across 43 different African countries (Figure 1), covering the wide diversity of climatic zones across Africa—from the warm Mediterranean climate of Algiers (Algeria) to the Equatorial climate of Douala (Cameroon) and the humid subtropical climate of Antananarivo (Madagascar). The total population of these cities for the year 2015—retrieved from the 2018 Revision of WUP (United Nations, 2018)—is 243 M, that is, ~53% of the continental urban population and ~21% of the total continental population.

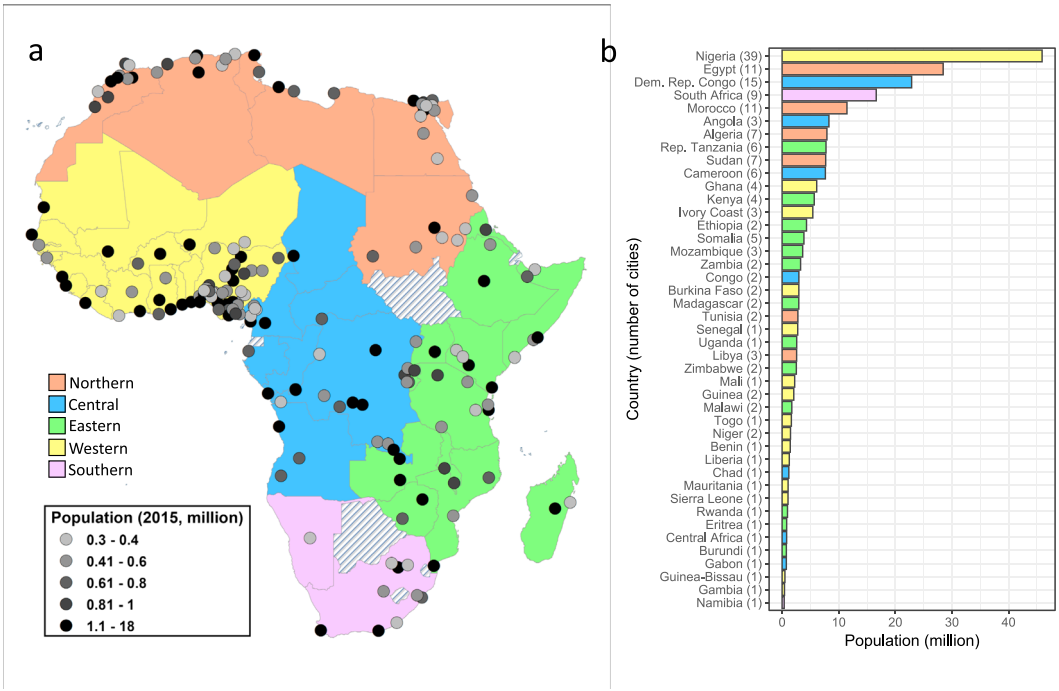

Figure 1. (a) Location of the 173 investigated cities with 2015 population (million), covering the five African regions; (b) sum of the population (million) for each country covered by the selected cities (countries not covered are dashed), with number of sample cities in each country.

2.2. Socioeconomic Scenarios and Urban Population Projections

Associated with major uncertainties, future socioeconomic trends must be approached with scenarios that span the wide range of plausible futures. Here we employed the five SSPs (O'Neill et al., 2017) in order to explore future population growth and urbanization under varying levels of socioeconomic development. Trends in population growth under the five SSPs were generated based on assumptions of changes in mortality, fertility, migration, and education (KC & Lutz, 2014, 2017) whereas trends in urbanization (i.e., ratio of urban/rural population) were developed separately using three urbanization pathways—fast, central, or slow (Jiang & O'Neill, 2017). Furthermore, assumptions in relation to the spatial pattern of urbanization under the SSPs were developed by Jones and O'Neill (2016); see Table 1.

We employed two separate approaches to project the future urban population size of the sample cities under the SSPs, namely, one spatial (SP) and one non-spatial (NS) approach (Figure 2a). The use of these two distinct approaches enabled us to account for uncertainties in both the modeling technique and the practical delimitation of cities' boundaries—based on administrative areas (NS approach) or on contiguity of the urban extent (SP approach).

Starting with the NS approach, we retrieved country-level population projections (KC & Lutz, 2014, 2017) and urbanization projections (Jiang & O'Neill, 2017), from which we derived the total urban population of each African country under each of the SSPs, from 2010 to 2100, in 5-year time steps. Employing the

Table 1
Main Assumptions of the Five SSPs for Population Growth, Urbanization Level, and Spatial Pattern of Urbanization

Variable	SSP1	SSP2	SSP3	SSP4	SSP5
Population growth	Low	Medium	High	High	Low
Urbanization level	Fast	Central	Slow	Fast	Fast
Spatial pattern	Concentrated	Historical patterns	Mixed	Mixed	Sprawl

Note. SSP = shared socioeconomic pathway. Under SSP4, population growth is "medium-low" for South Africa, Tunisia, Morocco, and Libya, and urbanization level is "central" for Equatorial Guinea.

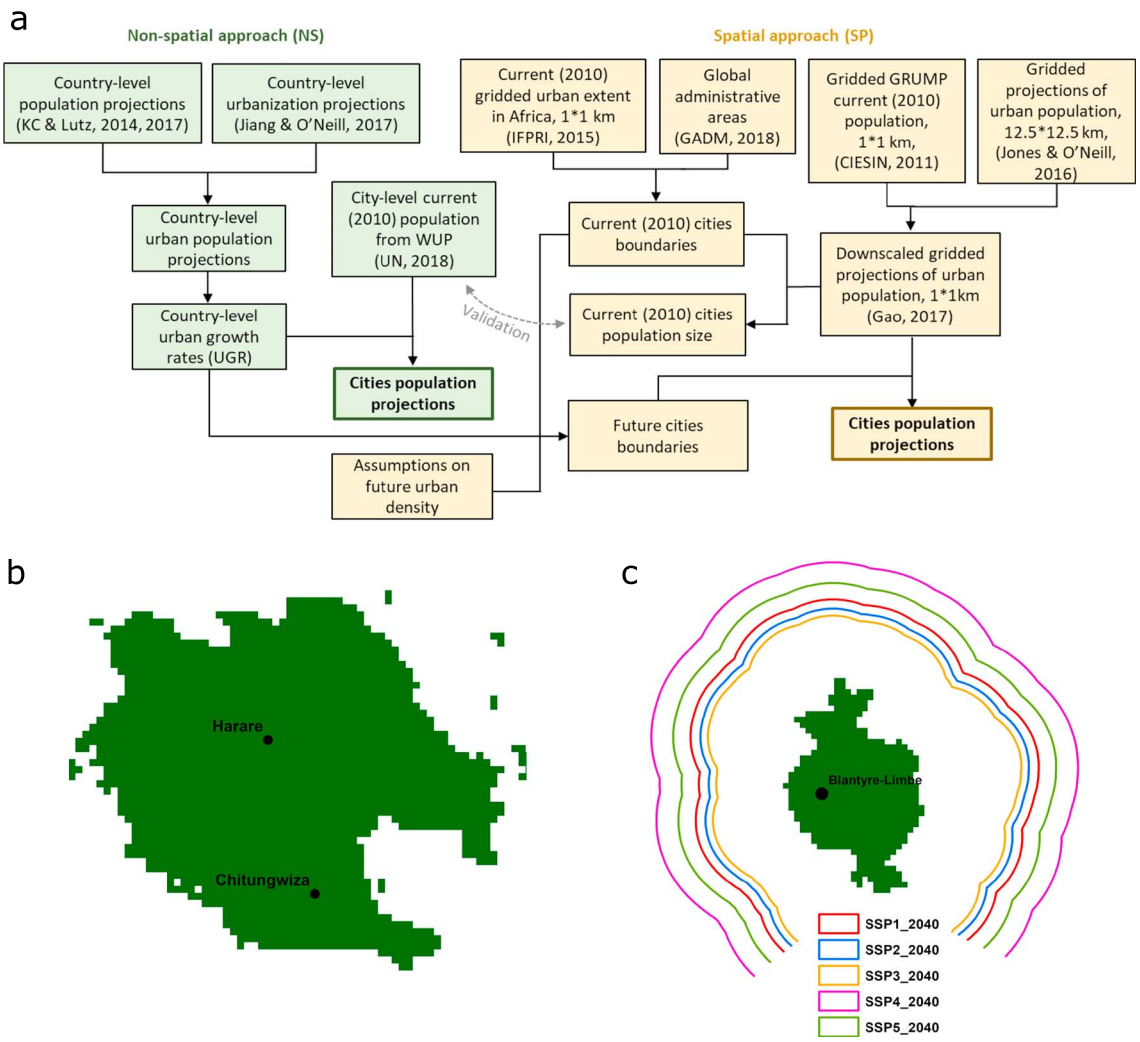

Figure 2. (a) Schematic workflow of the spatial (SP) and nonspatial (NS) approaches to compute cities population projections, repeated under each of the shared socioeconomic pathways for every 5- and 10-year time steps for the SP and NS approach, respectively; (b) example of cities that currently share a common urban extent (in green) and that were therefore merged into one unique urban area (here Harare-Chitungwiza, Zimbabwe); (c) example of future cities' boundaries (here Blantyre-Limbe, Malawi) under each of the shared socioeconomic pathways for the year 2040, based on assumptions of urban density and urban growth rates.

compound growth approach described by Hoornweg and Pope (2016), we then computed country-, SSP-, and time-specific urban growth rates (UGRs). Assuming that cities follow their respective country's UGRs, we applied the UGRs to the current cities' population figures (United Nations, 2018) and projected their future population size under the five SSPs, for each 5-year time steps (equation (1)). Such an approach enables accounting for the contribution of both endogenous demographic growth and in-migration from rural areas to the future city's population size.

$$City\_pop_{t+\Delta t} = City\_pop_t \left\{ 1 + \left[\left(\frac{Country\_pop_{t+\Delta t}}{Country\_pop_t} \right)^{\frac{1}{\Delta t}} - 1 \right] \right\}^{\Delta t}, \quad (1)$$

where *City _ pop* is the city's population size for a given time t, Δt is a 5-year time step, and *Country _ pop* is the country's urban population size for a given time t.

For the SP approach, we first delineated the current cities' boundaries by (i) using a 1-km spatial data set of urban extent for the year 2010 (IFPRI, 2015) and (ii) defining a city as a contiguous urban extent centered around its administrative area boundaries (GADM, 2018; Figure S1). Cities that shared a contiguous

urban fabric were merged into one, for example, the cities of Harare and Chitungwiza (Zimbabwe) were merged to form the urban area of Harare-Chitungwiza (Figure 2b). In this way, we merged 22 cities into 12 different urban areas (Table S2), thus shifting the final sample of investigated cities from 185 to 173. To enable the comparison of the population projections obtained with the SP and NS approaches, we aggregated the NS-based projections of the 22 aforementioned cities accordingly—for example, NS-based projections of Harare and Chitungwiza were summed to obtain the population projections of Harare-Chitungwiza.

Second, we employed the gridded projections of urban population described in Jones and O'Neill (2016)—and downscaled to a 1-km grid by Gao (2017) using the Global Rural-Urban Mapping Project grid (CIESIN, 2011)—to compute the size of the urban population contained within each city boundaries. We compared each city's population size obtained in this way with the WUP estimates (United Nations, 2018) for the same year (2010) and identified a large difference (>100%) between the two urban population figures for 38 cities (Table S3). For those 38 cities, we refrained from employing the SP approach—that is, population projections of those cities are based only on the NS approach.

Third, we delineated future cities' boundaries based on assumptions of urban expansion under each SSP. Recent findings suggest that Africa will show the highest rate of increase in urban land cover worldwide, with a roughly sevenfold increase in 30 years (Seto et al., 2012). Here we consider urban expansion as being a function of both urban population growth and decline in urban population density (Angel et al., 2016). Projections of urban population growth were directly retrieved from the UGRs computed in equation (1), while projections of decline in urban density were informed by historical trends (Angel et al., 2016), existing scenarios of urban densities in Africa (Angel et al., 2011; Guneralp et al., 2017) and assumptions of spatial patterns of urban development under the SSPs (Jiang & O'Neill, 2017; Jones & O'Neill, 2016). Based on these sets of information, we assumed no change in population density under SSP1 and an annual decline of (i) 1% under SSP2 (similar to the rate observed in Africa from 1990–2000), (ii) 1.5% under both SSP3 and SSP4 due to mixed spatial patterns of development, and (iii) 2% under SSP5 due to urban sprawling. Assuming a proportional relationship between urban expansion and its two drivers (Angel et al., 2011), both UGRs and annual % of decline in population density were then translated into country- and SSP-specific fold changes in size of urban area compared to the baseline (2010) conditions (equation S1 and Figure S2a). The resulting fold changes—dominantly driven by population growth, except under SSP5 in some regions (Figure S2b)—were then applied to the current cities' boundaries to determine their future boundaries under each SSP and time step, assuming a homogeneous urban expansion around the cities' centroid and defining large water bodies and national borders as barriers of urban expansion (Figure 2c). We merged into so-called mega urban regions (MURs) a number of nearby cities that presented overlapping boundaries due to urban expansion.

Finally, we employed spatially explicit projections (1 km) of urban population counts under the different SSPs and time steps (Figure S3) and computed the size of the urban population contained within each city boundary, for all SSPs and time steps. In the case of the MURs that were formed based on the overlap of cities' future boundaries, we broke down the MURs population projections into cities' population projections based on their respective population proportion within the MUR for the year 2010. This enabled the retention of the original sample of 173 cities.

2.3. Climate Scenarios and Heat Index Projections

Uncertainties in future greenhouse gas emissions are accounted for by three climate scenarios, namely, RCP2.6, RCP4.5, and RCP8.5. We employed a collection of 22 high-resolution regional climate models (RCM) runs from the multimodel CORDEX-Africa ensembles (Table S4), which have recently been used to explore future changes in climatic conditions across Africa (Weber et al., 2018), including heat waves (Dosio, 2017) and heat stress (Sylla et al., 2018). CORDEX-Africa runs are freely available through usual climate data nodes, with a spatial resolution of 0.44° (i.e., roughly 45 km). We retrieved historical data from 1981 to 2005 and projected data under the three RCPs from 2006 onward. We considered the nearest climatic grid points of each city to be representative of the cities' climatic conditions.

Although some recent studies have considered only maximum temperature to define the heat index (*HI*) without accounting for humidity, for example (Dong et al., 2015; Harrington & Otto, 2018; Liu et al., 2017), evidence suggests that humidity plays an important role in temperature discomfort and dangerous

heat and thus must be integrated into the construction of the *HI* (Coffel et al., 2018; Davis et al., 2016; Matthews et al., 2017; Mora et al., 2017), particularly in South America, Africa, and South Asia (Russo et al., 2017). Various heat metrics that include both temperature and humidity have been developed over the past few years, all performing well and rather similarly (Anderson et al., 2013; Matthews et al., 2017). Here we employed the apparent temperature (*AT*) and defined the annual *HI* as being the number of days for which the daily maximum *AT* exceeds a given threshold, being set at 105 °F (i.e., 40.6 °C). The latter is based on the U.S. National Weather Services (NWS) threshold of dangerous heat, widely used in the literature (e.g., Matthews et al., 2017; Russo et al., 2017). Although a fixed threshold was preferred to a relative threshold for the main exposure analysis—to ensure the consistency with past studies—we also explored future extreme heat using relative thresholds, set as the 95th, 97.5th, and 99th percentiles of the historical local maximum *AT*. To compute the *AT*, we employed the NWS equation (equation (2)) with adjustments when required (NWS, 2014).

$$AT = -c_1 + c_2T + c_3RH - c_4T.RH - c_5T^2 - c_6RH^2 + c_7T^2.RH + c_8T.RH^2 - c_9T^2.RH^2, \quad (2)$$

where *AT* is apparent temperature (°F), *T* is daily maximum air temperature (°F), *RH* is daily mean relative humidity (%), c_1= 42.379, c_2= 2.04901523, c_3= 10.14333127, c_4= 0.22475541, c_5= 0.00683783, c_6= 0.05481717, c_7= 0.00122874, c_8= 0.00085282, and c_9= 0.00000199.

While daily projections of maximum temperature were available for all RCM runs, projections of daily relative humidity were not always available. Where this was the case, we computed relative humidity based on daily projections of specific humidity, air temperature, and surface pressure (equation S2).

Data sets of observed daily climate variables (such as maximum temperature) for Africa are very scarce (Donat et al., 2013). Therefore, we employed the ERA-Interim (ERA-I) reanalysis from the European Center for Medium-Range Weather Forecasts (Dee et al., 2011) to evaluate the models' ability to reproduce historical *RH*, *T*, *AT*, and *HI* over the reference period (1981–2005). We (i) remapped ERA-I daily data to the RCM grid (0.44°) using bilinear interpolation; (ii) employed the hypsometric equation (equation S3) to compute the surface pressure from the mean sea level pressure, air temperature, and surface elevation; and (iii) subsequently computed daily *RH* and *AT*. Comparisons between the ERA-I reanalysis and the multimodel mean highlighted the latter's low ability to reproduce historical *RH*, *T*, and *AT* (Figures S4–S6). Conversely, multimodel mean *AT* based on the combination of models' *RH* and ERA-I *T* performed well (Figure S6), highlighting the dominating role that *T* plays in *AT*'s bias. We therefore bias corrected RCMs' daily *T*—using ERA-I reanalysis data sets and a quantile mapping approach with parametric transformations (Dosio, 2016)—and employed these bias-corrected projections of *T* to compute both historical and future *AT* and *HI*.

2.4. Exposure Assessment Framework

We defined exposure as being the number of people exposed to dangerous heat–that is, the annual *HI* (i.e., number of days when $AT > 40.6$ °C) multiplied by the number of people exposed (Jones et al., 2015). The unit of exposure is therefore person-days—in line with other studies (e.g., Coffel et al., 2018; Jones et al., 2018; Liu et al., 2017). For each city and each year, we computed the annual number of person-days of exposure to dangerous heat and averaged them over the baseline period (1985–2005) and future time periods, namely, the 2030s (2020–2040), the 2060s (2050–2070), and the 2090s (2080–2100). Exposure was computed under each climate model run and for both sets of urban population projections (SP and NS). We employed the multimodel mean to explore the results (one model being the combination of one climate model run and one set of population projections) and accounted for the intermodels variation through interquartile ranges (IQRs).

Considering that certain SSP*RCP combinations are very unlikely to arise (Kriegler et al., 2012), we discarded the few inconsistent combinations—SSP1*RCP8.5, SSP3*RCP2.6, SSP5*RCP2.6—and employed the remaining twelve potential SSP*RCP combinations (Table S5) to account for the full range of plausible futures and to allow for an exploration of the effect on exposure of different SSPs under a given RCP, and vice versa.

We also explored the individual influence of demographic and climatic changes on future exposure by computing the so-called climate effect, population effect, and interaction effect (Jones et al., 2015). The

climate effect is computed under each RCP by holding population constant (i.e., averaged over the historical period) while accounting for climate change. The population effect is computed under each SSP by holding the climate constant (i.e., averaged over the historical period) while accounting for demographic change. The interaction effect (i.e., change in exposure that results from simultaneous changes in both climatic and demographic conditions) is computed under all selected RCP*SSP combinations as the difference between the total exposure and the sum of the climate and population effects. It depicts change in exposure resulting from concurrent changes in climate and population. This metric is particularly relevant in that it captures and quantifies the process by which local populations move into harm's way, that is, grow and move into cities that are experiencing increasingly dangerous heat conditions.

Finally, we assessed the extent to which exposure was avoided as a result of shifts in socioeconomic or climatic pathways. We particularly focused on the decrease in exposure (in both absolute and relative terms) associated with shifts (i) from a high (or medium) to a low urban population growth pathway, under different climatic conditions (RCPs), and (ii) from a high (or medium) to a low radiative forcing pathway, under different socioeconomic conditions (SSPs) .

3. Results

3.1. Urban Population Projections

Based on the mean of the cities' population projections obtained with the SP and NS approaches, results show that the total population of the 173 sample cities increases under all SSPs compared to the current population (Figure 3a). SSP4 leads to the highest growth, with the total urban population reaching 1,230 (±232) M inhabitants by 2070 and 1,772 (297) M by 2100, that is, an approximately ninefold increase compared to the baseline (year 2010) population of 209 (31) M people. At the opposite end of the scale, SSP1 and SSP5 are the scenarios leading to the lowest growth, with total urban population reaching, respectively, 813 (150) and 891 (173) M people in 2100, that is, a roughly fourfold increase compared to the baseline. Results also show that under all scenarios—except SSP4—the pace of urban population growth will slow down as of circa 2060. Such continental-scale results hide a number of differentiated trends at the regional scale. Eastern and Western Africa are the regions showing the most significant growth under all scenarios, with the largest increase expected under SSP4. In the latter scenario, the urban population of the sample cities in Central, Western, and Eastern Africa will reach, respectively, 275 (19), 796 (173), and 514 (67) M people in 2100, meaning, respectively, an ~10-, 12-, and 17-fold increase compared to the baseline. Conversely, Northern and Southern Africa both show a relatively small increase, with an expected decrease in the second half of the century under certain scenarios (SSP1, SSP2, SSP4, and SSP5 in the case of Southern Africa and SSP1 and SSP5 in the case of Northern Africa).

Country-level results (Figure S7) emphasize the contrast between the fast-growing countries of Eastern and Western Africa (e.g., Kenya, Ethiopia, Niger, Malawi, Rwanda, and Uganda) and the slower-growing countries of Northern and Southern Africa (e.g., Egypt, Algeria, Gabon, Tunisia, and South Africa). As an example, the total population of the selected Malawian cities demonstrates an ~14- to 39-fold increase (depending on the SSP) by 2100 compared to the baseline, whereas the total population of selected Tunisian cities stabilizes or only doubles—depending on the SSP.

City-level results show that the five largest African cities in 2100 under a high urban population growth pathway (SSP4) are Lagos-Ikorodu (Nigeria), Kinshasa (Dem. Rep. Congo), Kampala (Uganda), Addis Ababa (Ethiopia), and Kano (Nigeria), with population attaining up to ~126 (18), 83 (3), 75 (19), 67 (9), and 58 (26) M inhabitants, respectively, under SSP4 (Table S6). Overall, the number of megacities drastically increases over Africa (Figure 3b), with the number of cities hosting more than 5 M inhabitants increasing from 5 (1) in 2010 to 63 (8) and 79 (9) in 2100 under SSP3 and SSP4, respectively. Similarly, while currently there are no megacities with more than 20 M inhabitants in our sample, projections show that between 6 (1) and 22 (3) megacities will be larger than 20 M inhabitants by 2100, depending on the urban population growth pathway.

The distinction between the endogenous demographic growth and the rural-urban migration shows that the contribution of these two drivers differs widely across SSPs, time steps, and countries (Figure S8)—as depicted in the SSPs' narratives. Under SSP4 and SSP5, urban population growth in fast-growing cities

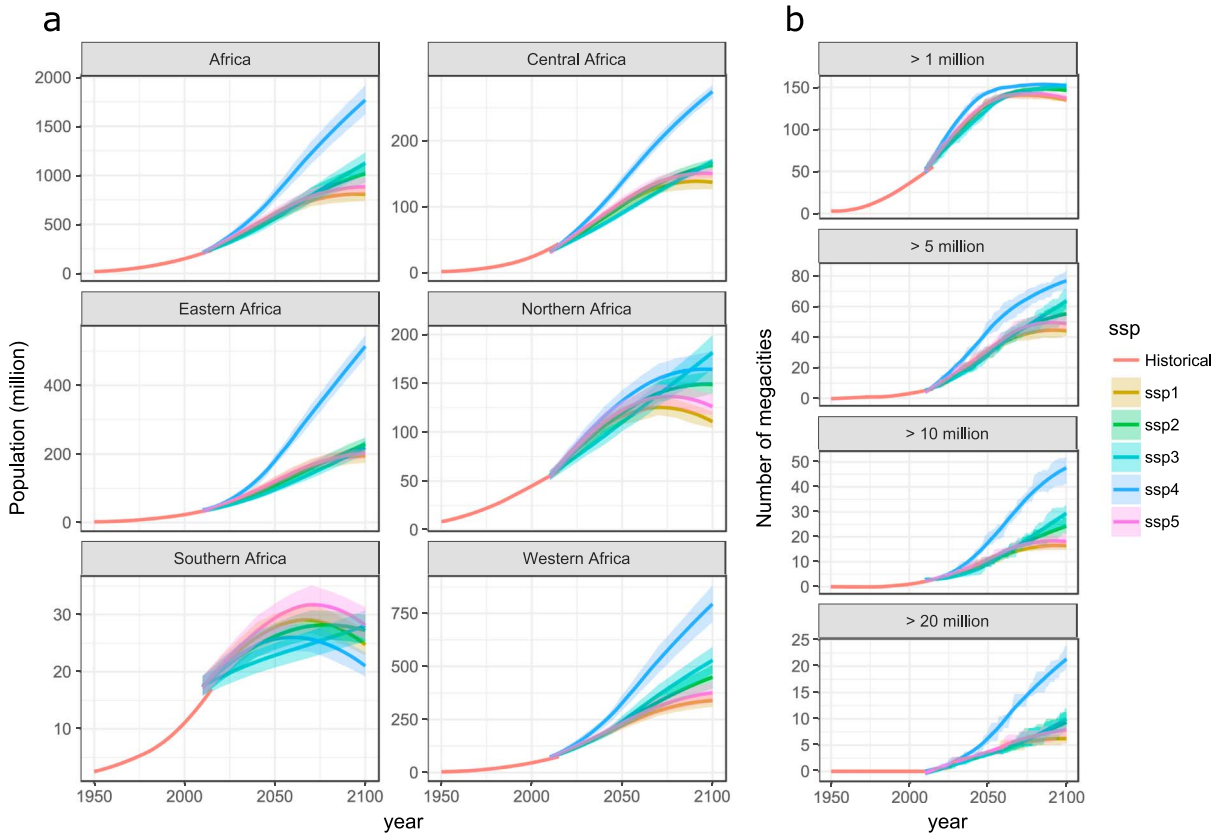

Figure 3. (a) Population projections (in million people) of the cities investigated, summed for the whole continent and per region, under the five shared socioeconomic pathways (SSPs); (b) projections of the number of megacities (with different thresholds of population size) for the whole continent, under the five SSPs. Shaded areas represent the range of the two modeling approaches.

(e.g., cities of Burundi, Burkina-Faso, Eritrea, Kenya, or Rwanda) is predominantly driven by rural-urban migration, particularly toward the second half of the century. Conversely, urban population growth is mainly driven by endogenous demographic growth under SSP1, SSP2, and SSP3, particularly in slower-growing cities.

3.2. HI Projections

At the continental level, the multimodel mean *HI* (i.e., annual number of days when the maximum *AT* exceeds 40.6 °C) averaged over the investigated cities increases under all RCPs until the 2060s and then stabilizes at around 59 (IQR = 27) and 82 (36) days/year by the 2090s under RCP2.6 and RCP4.5, respectively (Figure 4a). Conversely, the *HI* continues to rise under RCP8.5 to reach 123 (47) days/year on average by the 2090s, meaning an ~3.5-fold increase compared to the historical period (1985–2005). Regional results indicate that the cities of Western Africa are by far the most severely affected by dangerous heat, with a projected *HI* reaching 145 (60) and 196 (62) days/year by the 2090s under RCP4.5 and RCP8.5, respectively. Even under a scenario of low radiative forcing (RCP2.6) the mean *HI* of Western African cities will be higher than the regional mean *HI* of other regions' cities under high radiative forcing (RCP8.5). Noteworthy, results also show that the number of cities nearly unaffected by dangerous heat (*HI* < 5 days/year) will rapidly decrease, shifting from 56 (17) in the historical period to 30 (12) by the 2060s to 20 (11) by the 2090s under RCP8.5 (Figure 4b), that is, only ~11% of our sample. Similarly, the number of cities experiencing dangerous heat during more than 200 days/year considerably increases under RCP8.5, reaching no less than ~24% of our sample by the 2090s, compared to ~1% over the historical period. It is also worth noting that lower-end scenarios (RCP2.6 and RCP4.5) substantially limit the occurrence of extreme *HI* (e.g., >250 days/year) —with less than ~4% of the selected cities being concerned by the 2090s under these scenarios—in contrast with RCP8.5, under which ~17% of the sample cities are affected by extreme *HI*. In line with the regionally

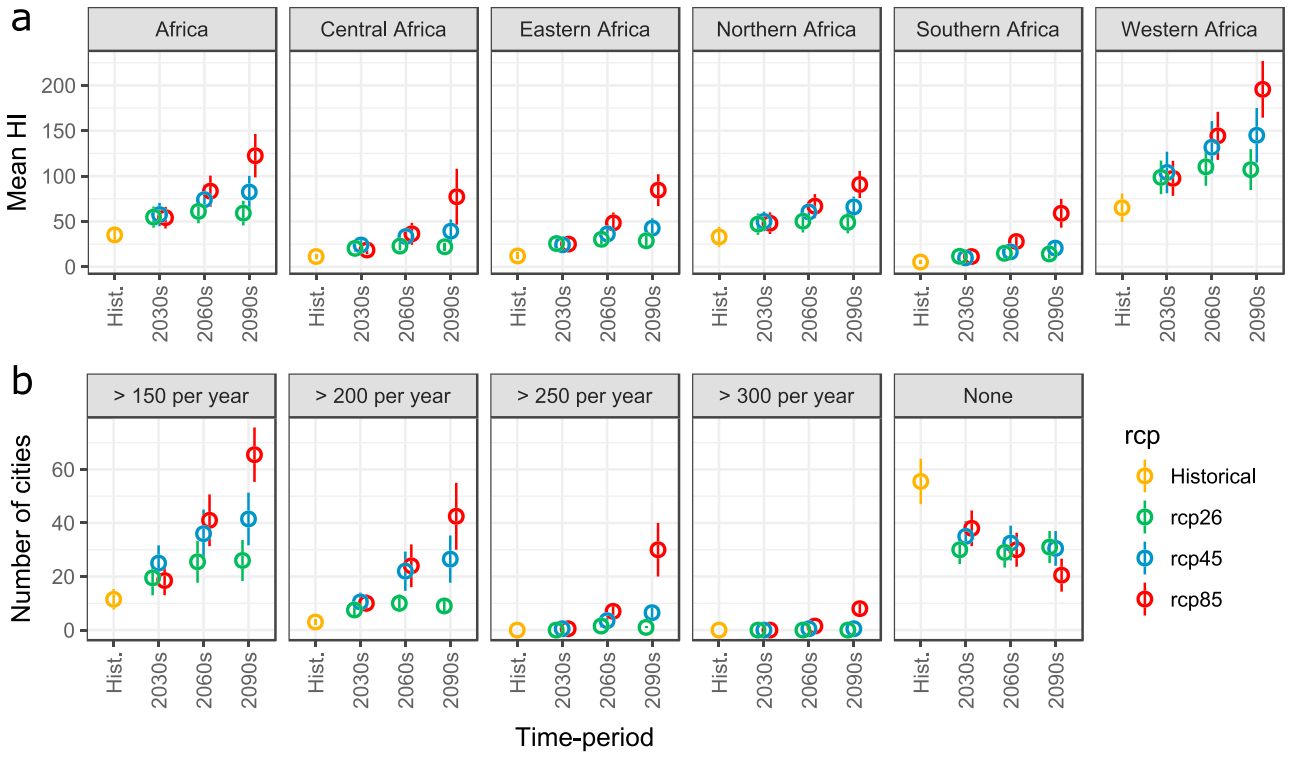

Figure 4. (a) Projections of HI averaged over the continent or regions under different representative concentration pathways and time periods; (b) projections of the number of cities that exceed a given mean HI threshold, under different representative concentration pathways and time periods. Error bars represent the inter-quartile ranges of the climate models' simulations.

aggregated projections, country- and city-scale results (Figures S9 and S10) showed that the most affected countries and cities are located in Western Africa, with several cities of Benin, Burkina Faso, Mali, Guinea-Bissau, and Ghana showing extreme *HI* (>250 days/year) by the 2090s under RCP8.5. The *HI* sensitivity to scenarios is highly dependent on the region and cities. Some cities show a *HI* of the same magnitude under all RCPs—for example, the *HI* of Niamey (Niger) in the 2090s is between 189 (29) and 225 (31) days/year—whereas other cities such a Luanda and Lubango (Angola) show *HI* values by the 2090s that are ~2.5 times less under RCP2.6 than under RCP8.5.

3.3. Exposure Projections

During the historical period (1986–2005), exposure to dangerous heat—aggregated at the continental level (i.e., sum of exposure of all the investigated cities)—was on average 4.2 (IQR = 0.9) billion person-days per year. Our projections (Figure 5a) show that this figure will increase under all scenario combinations, reaching from 20 (6) to 26 (7) billion person-days per year in the 2030s, from 45 (39) to 95 (25) in the 2060s, and from 86 (33) to 217 (66) in the 2090s, depending on the scenario combination. For the end of the 21st century, such figure represents a 20- to 52-fold increase in exposure compared to the historical period.

As one would expect, the lowest increase in exposure is expected under the combination of a low-end climate scenario (RCP2.6) with a socioeconomic scenario depicting slow population growth and concentrated urbanization (SSP1), whereas the highest increase in exposure is expected under a high-end climate scenario (RCP8.5) combined with a high population growth and fast urbanization, as depicted under SSP4. Projections of exposure aggregated at the continental scale for the other possible scenario combinations lie in between these two plausible futures. Exposure projections also showed little variability across scenario combinations in the 2030s and the 2060s, compared to that in the 2090s. As an example, variability of exposure—aggregated at the continental level—across scenario combinations is of ~52 and ~166 billion person-days in the 2060s the 2090s, respectively. Such an increase in the variability of outcomes toward

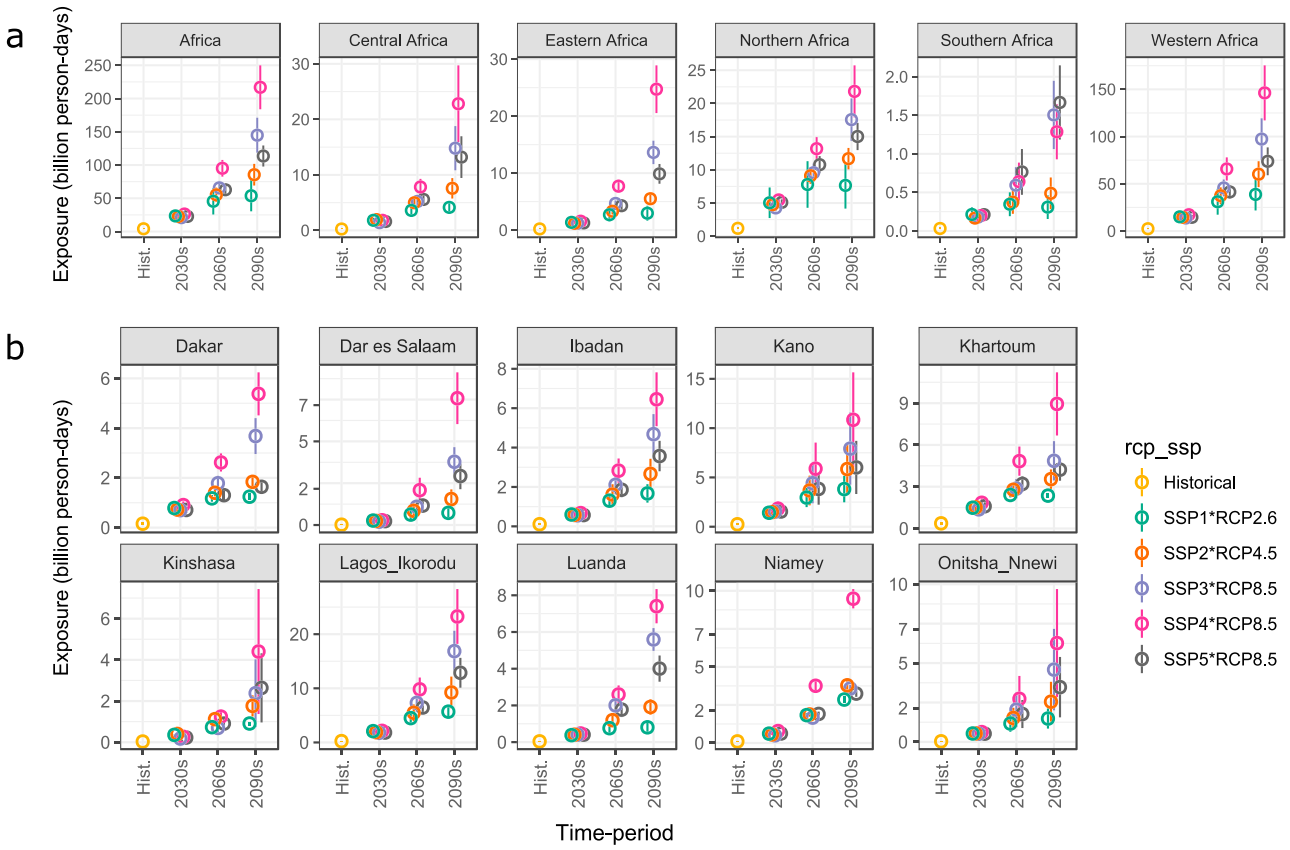

Figure 5. Projections of exposure (in billion person-days) averaged over different time horizons, (a) for the whole continent and regions and (b) for the 10 most exposed cities. Error bars represent the interquartile ranges.

the end of the century is even more pronounced in Central and Eastern Africa, where variability across scenario combinations is ~4.5 times greater in the 2090s than in the 2060s.

Results also showed that exposure is unevenly distributed across the African continent, with the most affected region—in absolute terms—being Western Africa (Figure 5a), due to numerous and highly populated urbanized areas and to increasing extreme temperature events. In this region, Nigeria suffers the most, as it makes up ~3/4 of the regional exposure (Figure S11) due to its high number of large cities (39 were included in our sample). Thanks to a slow—and partially decreasing—urbanization and population growth as well as to a milder climate, Southern Africa remains relatively unscathed, with a mean annual exposure of less than 2 billion person-days per year in the 2090s under all scenario combinations. In relative terms, Eastern and Central Africa exhibit the highest increase in exposure, reaching, respectively, 119- and 89-fold by the 2090s under SSP4*RCP8.5, whereas exposure in other regions increases by less than 60 times the historical figure under all scenario combinations.

A closer look at the city level (Figure 5b and Figure S12) revealed that Lagos-Ikorodu (Nigeria), Niamey (Niger), Kano (Nigeria), Khartoum (Sudan), and Luanda (Angola) are the five most exposed urban areas by the 2090s, under most scenario combinations. In the worst-case scenario (SSP4*RCP8.5), the mean annual exposure in Lagos-Ikorodu will reach 23 (10) billion person-days per year by the 2090s, compared to 0.25 (0.15) billion person-days per year during the historical period. Among the five most exposed cities, Luanda exhibits the highest increase in relative terms compared to the historical period, increasing 181-fold under SSP4*RCP8.5 by the 2090s. Under the same scenario combination, a number of Eastern African cities show a striking 2,000-fold increase in exposure compared to the historical period, for example, Blantyre-Limbe (Malawi), Lusaka (Zambia), Kampala (Uganda), Likasi, Kolwezi, and Lubumbashi (Rep. Dem. Congo), highlighting the new emergence of dangerous heat conditions in these areas.

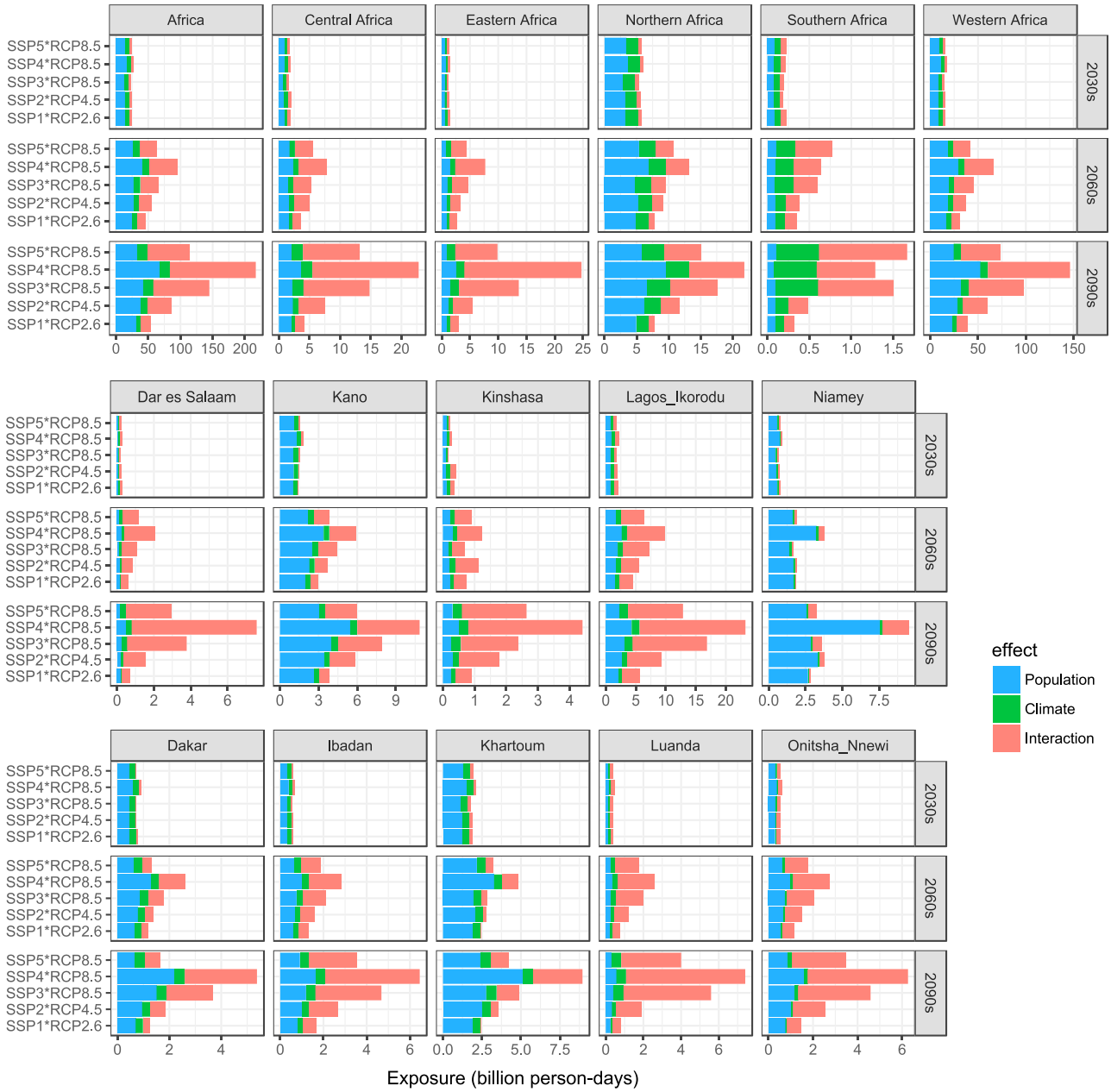

Figure 6. Population, climate, and interaction effect under five selected combinations of SSP*RCP, by the 2030s, 2060s, and 2090s, for Africa, the five African regions, and the ten most exposed cities. SSP = shared socioeconomic pathway; RCP = representative concentration pathway.

3.4. Climate, Population, and Interaction Effects

Combining both historical figures and projections of urban population and dangerous heat, we assessed the individual contribution of changes in climatic and socioeconomic conditions—respectively, the population and climate effect—as well as the interaction effect (Figure 6). Results showed that at the continental level, exposure to dangerous heat is primarily driven by the population and interaction effects, with the climate effect alone being negligible in all cases, meaning that climate change has limited influence on future exposure if not accompanied by urban population growth. At the regional level, all regions follow similar patterns, excepting Northern Africa (to some extent) and Southern Africa, for which the climate effect plays a substantial role (particularly under RCP8.5), partly due to the relatively limited urban population growth expected in these regions. Eastern Africa shows the highest interaction effect, highlighting the synergistic

interaction between the emergence of frequent dangerous heat—that was rarely experienced during the historical period—and rapid urban population growth. Dar es Salaam (Tanzania) clearly illustrates the interaction effect. While this city is not exposed to extreme heat conditions in the historical period and in the 2030s, the occurrence of such extreme conditions by the 2090s (under RCP4.5 and RCP8.5) combined with steady urban population growth will make Dar es Salaam one of the tenth most exposed cities by the end of the century (reaching 7.6 (3.1) billion person-days per year in the worst-case scenario). Conversely, future exposure in Western African cities such as Niamey (Niger) and Kano (Nigeria) is predominantly driven by the population effect (explaining between 65% and 98% of the multimodel mean exposure), due to the relatively low increase in the occurrence of dangerous heat conditions—which was already high in the historical period—compared to the fast and continuous increase in urban population expected under all SSPs.

3.5. Avoided Exposure

Results aggregated at the continental level showed that a shift from a high (SSP4) to a low (SSP1) urban population growth pathway would reduce exposure by ~51% (IQR = 12) in the 2090s (Figure 7), regardless of the climatic conditions. This is slightly higher than the reduction in exposure triggered by a shift from a high (RCP8.5) to a low (RCP2.6) radiative forcing pathway, which is of ~48% (13) by the 2090s, regardless of the socioeconomic conditions. In absolute terms (Figure S13), a shift from SSP4 to SSP1 under RCP8.5 or RCP4.5 would reduce exposure by ~108 or ~78 billion person-days per year in the 2090s, whereas a shift from RCP8.5 to RCP2.6 under SSP4 or SSP2 would reduce exposure by ~103 or ~62 billion person-days per year.

The extent to which a shift in socioeconomic pathways has a larger potential for reduction in exposure than a shift in radiative forcing pathways is very dependent on the time periods, cities, and pathways considered. In Western Africa, the shifts in SSPs are more influential than shifts in RCPs for 83% of the cities. In this region, even a moderate shift from a high (SSP4) to medium (SSP2) urban population growth pathway leads to a greater reduction in exposure than a shift from RCP8.5 to RCP2.6, emphasizing the dominant role that socioeconomic pathways play in Western Africa. Conversely, in other highly exposed regions such as Central and Eastern Africa, shifts in RCPs have a slightly greater influence than shifts in SSPs, particularly for the midterm (2060s) horizon. In the 2090s, however, shifts from high to low or high to moderate urban population growth pathways in Eastern Africa would lead to a larger reduction in exposure than a shift from RCP8.5 to RCP4.5. In cities where the population effect was found to be particularly high (e.g., Niamey, Niger), the reduction in exposure by the 2090s due to a SSP4-SSP1 shift is ~4 times larger than the reduction due to a RCP8.5-RCP2.6 shift (~65% vs. ~17%).

It is important to note here that a significant part of the avoided exposure due to shifts in urban population growth pathways is a result of the slowdown in rural-urban migration depicted in most low urban population growth pathways. In that case—provided similar climatic conditions, which is unlikely to be the case considering urban microclimate—the burden of exposure is in fact not avoided, but rather relocated elsewhere outside of the cities.

4. Discussion

4.1. Diversity of Outcomes

We have shown in this paper that exposure to dangerous heat in African cities will gradually increase throughout the 21st century to reach 86–217 billion person-days per year in 2090s at the continental level, meaning a 20- to 52-fold increase compared to the historical period. Exposure will increase unevenly across the African continent, with most Western and Eastern African cities showing the largest increase in absolute and relative terms, respectively. Exposure to dangerous heat in megacities located in tropical areas such as Kinshasa (Rep. Dem. Congo), Kano (Nigeria), and Lagos-Ikorodu (Nigeria) is likely to exceed 3, 5, and 10 billion person-days per year, respectively, by the 2090s.

Employing 12 different SSP*RCP combinations, we explored the multitude of plausible futures and demonstrated that these yield levels of exposure that are (i) rather similar by the 2030s and the 2060s and (ii) very different in the 2090s. The low variability in outcomes across SSP*RCP combinations during the first half of the century sheds light on the unavoidable increase in exposure to extreme heat that African cities will experience in the next decades. Considering the high confidence in midcentury exposure projections,

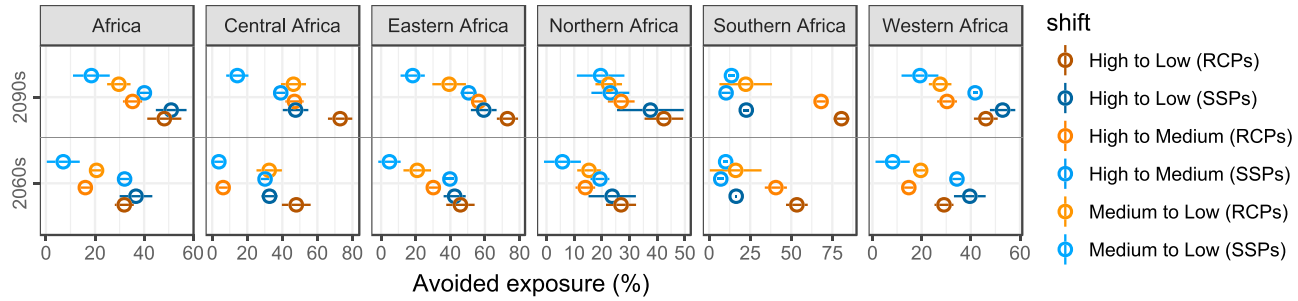

Figure 7. Relative reduction in exposure (%) triggered by shifts in representative concentration pathways (RCPs; high = RCP8.5; medium = RCP4.5; low = RCP2.6) and by shifts in shared socioeconomic pathways (SSPs; high = SSP4 [SSP5 for Southern Africa]; medium = SSP2 [SSP1 for Southern Africa]; low = SSP1 [SSP4 for Southern Africa]). Error bars represent the interquartile ranges. Note that the relative reduction of shifts in SSPs is similar under all RCPs, and the relative reduction of shifts in RCPs is similar under all SSPs.

local policy-makers must start taking actions now to build urban resilience and to adapt to the inevitable increase in exposure throughout the next 40–50 years. At the same time, global climatic and socioeconomic pathways play a crucial role in shaping future levels of exposure toward the end of the century. As an example, in Western Africa exposure could reach 146 (46) billion person-days per year by the 2090s in the case of a high urban population growth pathway combined with a high-end climate pathway (SSP4*RCP8.5) but could also be limited to 39 (33) billion person-days per year in the case of a limited urban population growth pathway combined with a low-end climate scenario (SSP1*RCP2.6). Such a large range of possible outcomes highlights the direct implications that climate mitigation policies—limiting emissions to reach the level of radiative forcing depicted under RCP2.6—and population and adaptation policies—limiting urban population growth and increasing adaptation as depicted under SSP1—have on future exposure to dangerous heat.

4.2. Sources of Uncertainty

The diversity of possible outcomes in future exposure to dangerous heat becomes even greater when considering the uncertainty associated with climate model simulations and population modeling approaches. While employing several climate models run is a common practice in climate impact assessments, using different sets of population projections is not. In this study, we accounted for the uncertainty both in climate models simulation and in population modeling approaches. To explore these two sources of uncertainty separately, we computed the yearly exposure for all climate model runs with each set of population projections separately. Aggregated at the continental and regional scales, results (Figure 8) showed that the uncertainty in exposure due to the climate model simulations (represented here by the IQR) is wider than that related to the population modeling approaches in Central, Eastern, and Southern Africa. In the two former regions, this can be explained by the minimal difference across the population modeling approaches (see Figure 3a) as well as by the fairly wide climate spread under RCP8.5—in Central Africa only (see Figure 4a). In Southern Africa, the large uncertainties in exposure due to climate model simulations are primarily related to the significant effect of climate change on exposure in this region, as shown by its substantial climate effect (see Figure 6).

Conversely, in Western and Northern Africa as well as at the continental level, the uncertainty related to the choice of the population modeling approaches is greater than that due to the climate model simulations, particularly under SSP3 and SSP4. This is mostly explained by (i) the significant population effect in these regions and (ii) the large differences in urban population projections across the two modeling approaches (see Figure 3a). Compared to the SP approach, the NS approach generally leads to higher urban population projections—particularly in already highly urbanized areas such as Western and Northern Africa—mainly because it assumes that (i) large cities will show a similar urban population growth rate to the national figure, (ii) there is no limit in population density—unlike the underlying population projections employed in the SP approach (Jones & O'Neill, 2016), which employed population density thresholds—and (iii) there are no barriers to growth (i.e., no adjacent cities, no country borders, and no natural barriers).

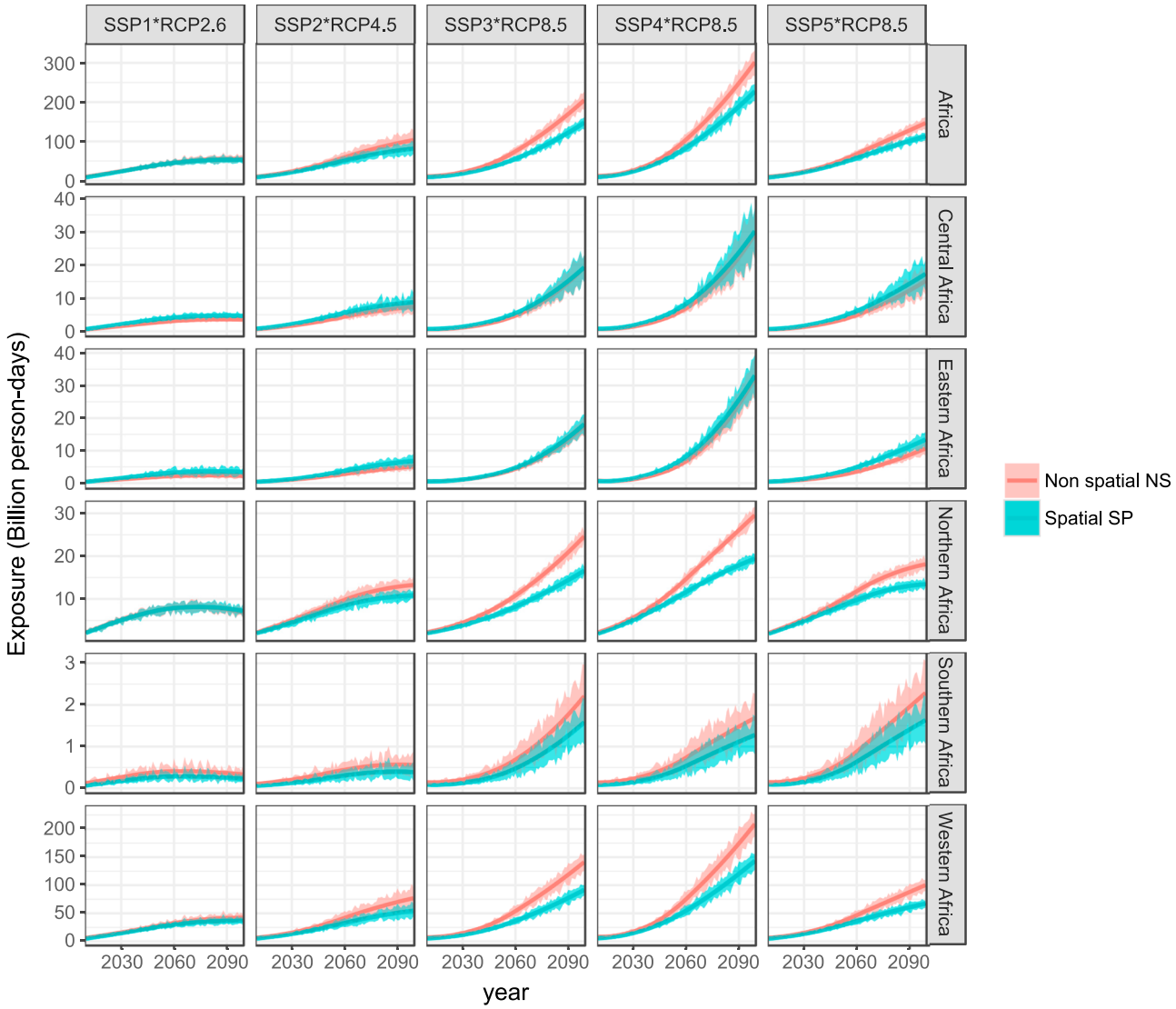

Figure 8. Yearly exposure (smoothed) in billion person-days, aggregated at the continental and regional scale, for five selected SSP*RCP combinations, computed separately for the nonspatial (NS, red) and spatial (SP, blue) population modeling approaches. Shaded areas display the interquartile ranges of the climate model simulations. SSP = shared socioeconomic pathway; RCP = representative concentration pathway.

4.3. Crucial Role of Societal Pathways

We further investigated the individual effect of changes in socioeconomic and climatic conditions by disaggregating the exposure projections into the climate, population, and interaction effects. Existing studies on heat exposure under the SSPs—which focused on the global or regional levels—all found the population effect to be significant, although more often than not lower than the climate and interaction effects (Asefi-Najafabady et al., 2018; Coffel et al., 2018; Jones et al., 2018; Liu et al., 2017). Here we corroborate the significance of the population effect and demonstrate that it is much higher than the climate effect alone—and of same magnitude as the interaction effect—in the context of African cities. This holds true under most time periods and scenario combinations. Compared to the global or regional scales, demographic change in African cities is of such magnitude that it has the potential to outweigh changes in climatic conditions alone, meaning that when not combined with urban population growth, the increase in extreme-heat events has limited effect on future exposure to dangerous heat in most cases. Such a finding stresses the important role that urban population growth and societal pathways more broadly play in shaping future exposure to dangerous heat in African cities. We explored this role further by comparing the

extent to which exposure could be avoided through shifts in socioeconomic or climatic pathways. The few existing studies that performed similar analysis found that a shift from a high to a low radiative forcing pathway led to greater reduction in exposure than a shift from a high to a low population growth pathway. This holds true at the global scale (Jones et al., 2018) but also (i) in the United States, where Jones et al. (2015) found that a shift to a lower emission pathway or to a lower population growth pathway would reduce exposure by ~56% and ~45%, respectively; (ii) in India, where Mishra et al. (2017) showed that a shift from high to low population growth has a lower influence on exposure than a shift from +2 to +1.5 °C; (iii) in Eastern Africa, where Harrington and Otto (2018) found that shifting from +2 to +1.5 °C would reduce exposure by ~81%, whereas shifting from a medium (SSP2) to low (SSP1) population growth pathway would reduce exposure by ~28%; and (iv) in North Africa/Middle East and Sub-Saharan Africa, where Jones et al. (2018) demonstrated that a shift from a high (SSP3) to low (SSP5) population growth pathway would lead to a lesser reduction in exposure than a shift from a high (RCP8.5) to low (RCP4.5) emission pathway (~33–39% vs. ~47–57%). Our results—while not entirely comparable because based on different population projections, HI, and scenarios range—differ slightly from those found in the literature in that a shift from a high to a low urban population growth pathway leads to a slightly greater reduction in exposure than a shift from a high to a low emission pathway (~51% vs ~48%). In other words, comprehensive socioeconomic and urban growth policies that would trigger the transition from a highly populous, urbanized, and regionally divided world (SSP4) to a less populous and highly equitable world (SSP1) may have the same influence on reduction in exposure to dangerous heat—at the continental scale—than very ambitious mitigation that would contain the global radiative forcing as low as RCP2.6 (instead of RCP8.5).

The fact that we found the role of demographic change to be more influential than in existing studies is due to three different factors. First, we applied a fixed threshold ($AT > 40.6$ °C) to compute the *HI*, whereas some of the existing studies employed relative thresholds (e.g., Coffel et al., 2018). When computed based on relative local thresholds of *AT* instead of a fixed threshold, the *HI* differs significantly (Figure S14), particularly in regions where relative local thresholds are low (e.g., Southern and Central Africa) or very high (e.g., above 50 °C). In most regions, the increase in a relative threshold-based *HI* from the historical to the future time periods is from 2 to 10 times larger than that of the fixed threshold-based HI (Figure S15), hence resulting in a much stronger climate effect. Second, this study focuses on a particular type of environment—African cities—whereas existing studies considered a regionally (or globally) contiguous space. Since African cities are highly populated and are experiencing one of the highest population growth worldwide, the population effect in such areas is inevitably larger than it is in less-populated and slower-growing regions. Third, we made use of the full range of SSPs—including a scenario of fast urbanization and high population growth (SSP4)—whereas existing studies usually employed a subset of the five SSPs, for example, SSP1/SSP2 in Harrington and Otto (2018). Using the five SSPs and/or including SSP4 (in the context of population growth in cities of developing countries) in the exposure assessment leads to a substantially larger difference in population outcomes—which partly determines the influence of shifts in SSPs on avoided exposure—than that of studies using less contrasted SSPs.

It should also be noted that the degree to which we find the influence of demographic change on avoided exposure to be higher than that of climate change depends on the cities and scenarios considered. While the influence of socioeconomic pathways is reinforced in Western African cities—where the range of outcomes in future urban population size is much wider than the range of outcomes in dangerous heat conditions (which are already high in the historical period)—it is of slightly lesser influence in Central and Eastern African cities where major changes in both urban population and dangerous heat are expected, and of minimal influence in Southern African cities where urban population growth is rather limited under all scenarios.

4.4. Vulnerability Under the SSPs

African cities' societal trajectories are not only important because they strongly influence future exposure to dangerous heat—through urban population growth—but also because they shape future vulnerability of the urban populations (Rohat, 2018). Although we refrained from including vulnerability in this paper—as it is hardly quantifiable in a data-poor environment—we acknowledge the crucial role that it plays in leveraging future heat-related health risks in urban areas (IPCC, 2012) and altering mortality outcomes of extreme heat events in Africa (Burkart et al., 2014). Just as they lead to differing urban population sizes, the

different SSPs lead to varying degrees of vulnerability, which has been shown to evolve over time (Rohat et al., 2019; Sheridan & Allen, 2018). SSP1, depicting a world with high education, investments in health, social cohesion, effective institutions, and rapid development and transfer of technology, would eventually lead to low vulnerability of African urban populations, further reducing the burden of heat-related health risks, already limited due to a slow urban population growth. In contrast, SSP4, depicting unequal health investments and access to health facilities, low social cohesion and participation, low and unequal economic growth, and inefficient institutions for the non-elites, would likely lead to a strong increase in vulnerability of African urban dwellers, worsening further heat-related health risks, already high to due to an exponential urban population growth.

4.5. Caveats

In addition to the specific limitations associated with the datasets that we employed—that is, the urban extent delineations (IFPRI, 2015), the WUP estimates (United Nations, 2018), and the downscaled urban population projections (Gao, 2017)—our two urban population modeling approaches also have their own drawbacks. Assuming that all the cities of a given country will share similar urbanization and population growth rate (under a given SSP), we neglected the different population dynamics of small-, middle-, and large-size cities (Birkmann et al., 2016). In addition, we excluded all drivers of urban population growth other than urbanization and demographic change, whereas recent research suggests that cities' growth is highly correlated with private capital investment and that megacities need to be underpinned by mega-economies, which might not be the case for a number of African cities under some SSPs (Satterthwaite, 2017a). Future population projections that (i) account for both demographic and economic components (Li et al., 2019) and (ii) consider thresholds of population density and urban expansion—informed by spatial data on national borders, water bodies, slope, land cover, and protected areas—will likely improve our estimates of future urban population size.

Another important component that is missing from our analysis is the urban heat island (UHI), which greatly increases surface temperature in the inner city—and in surrounding slums—during heat waves (Zhao et al., 2018), particularly in megacities (Papalexiou et al., 2018). Our estimates of exposure are therefore considered as conservative, as recent research suggests that the UHI—even under its current form—substantially increases future levels of exposure (Jones et al., 2018). Including the UHI in our analysis would be particularly useful to quantify the difference in heat exposure between urban and rural populations and to explore the impact of rural-urban migration on future exposure to extreme heat at the city scale. Nevertheless, accounting for the UHI in our analysis would require quantitative information on future urban land cover and morphologies under varying levels of socioeconomic development. While this has been achieved in a few local case studies (Houet et al., 2016; Lemonsu et al., 2015), it has yet to be conducted on a larger scale (e.g., multiple cities of a given region or continent) and in a data-poor environment.

In addition, even though our sample of cities comprises ~53% of the current continental urban population and covers a wide range of city size across 43 different countries, it does not include cities with less than 300,000 inhabitants and is therefore biased toward large cities. Nonetheless, small and intermediate urban centers are likely to face similar heat-related health challenges to larger cities, as the former also showcase a fast urban population growth and deficits in urban infrastructure and governance (Birkmann et al., 2016; Satterthwaite, 2017b; Wisner et al., 2015).

Furthermore, the reliability of the HI that we employed is subject to a number of caveats. Combining daily maximum T with daily mean RH to compute AT may result in an overestimation of the HI, as maximum T typically occurs when RH is at its lowest value. Ideally, AT should be computed from daily maximum T combined with daily minimum RH—or at best with simultaneous RH—but such data are currently unavailable within the CORDEX-Africa climate simulations. In addition, by applying a fixed threshold ($AT > 40.6$ °C) to compute the HI, any increase in AT over the threshold becomes irrelevant to our exposure assessment. This hinders the analysis of more extreme values of AT, which are for instance associated with extreme danger (when $AT > 54$ °C). Due to the lack of epidemiological and in situ evidence of heat-related mortality in Africa (Gasparrini, Guo, Hashizume, Kinney, et al., 2015; Gasparrini, Guo, Hashizume, Lavigne, et al., 2015; Gasparrini et al., 2017; Guo et al., 2018; Mora et al., 2017), it remains difficult to define appropriate local thresholds. Finally, the HI that we employed also does not account for the duration of the

extreme heat event and for the minimum temperature during the night, which are both important determinants of heat-related health impacts (Li et al., 2015).

5. Conclusion

Provided with estimates of future exposure under varying climate and socioeconomic scenarios, policy-makers can already grasp the extent to which urban populations will be impacted by dangerous heat in African cities, as well as pinpoint the kind of socioeconomic pathways that should be favored in order to mitigate heat-related health risks. Findings of this study therefore (i) raise awareness about the potential cobenefits—in terms of decrease in exposure to dangerous heat in urban areas and decline in vulnerability—of shifting toward a more sustainable, less populous, and less urbanized world; (ii) underline the necessity to mainstream climate change impacts and adaptation into spatial planning and urban development plans; and (iii) call for the integration of population and urbanization policies into the wide range of potential climate adaptation options (Bongaarts & O'Neill, 2018) at the urban scale (Sheridan et al., 2012). Examples of such policies include educational and health investments to stimulate the demographic transition (KC & Lutz, 2017), incentives to establish economic activities in rural areas and to favor the growth of secondary cities (OECD, 2016; United Nations, 2016), and the strengthening of urban-rural linkages (UN-Habitat, 2015). Further studies focusing on a specific city and/or region would be better positioned to provide more concrete and context-based adaptation strategies to reduce future exposure to extreme heat (Filho et al., 2018). Particular attention should be paid to strengthening the implementation of adaptation strategies at the urban scale, which is often poor due to weak governance (Pelling et al., 2018).

Further research is also needed to refine estimates of future heat-related health challenges, mainly by the use of improved methodologies to project future urban population growth—informed by projections of other socioeconomic parameters such as GDP and by a better delineation of future urban boundaries that account for geographic constraints such as slope, land cover, and protected areas—and by considering the current and future UHI and its influence on AT under different socioeconomic and climatic pathways (Georgescu et al., 2014). Future work should also aim at better characterizing the share of the population that is truly exposed to extreme heat—moving toward personal heat exposure research, which accounts for both indoor and outdoor environment and individual behaviors (Bernhard et al., 2015; Kuras et al., 2017). Finally, further research is certainly needed to go beyond exposure and to explore future vulnerability to heat under the different SSPs—employing the growing body of literature that extend and quantify the global SSPs' narratives (e.g., Crespo Cuaresma et al., 2018; Kurniawan & Managi, 2018; Witmer et al., 2017)—and particularly their ability to shift the burden of heat-related health risks in African cities to lower levels, under varying degrees of exposure.

Acknowledgments
This work was partly supported by the State Secretariat for Education, Research, and Innovation (SERI, Switzerland) within the framework of its program "Cotutelles de these" and by the Swiss National Science Foundation's Doc. Mobility scholarship. The authors declare no known conflict of interest and wish to thank Juliet Wilson for proofreading services as well as the three anonymous reviewers for their comments that helped improve the paper. The ERA-I climate reanalysis data were retrieved from the European Center for Medium-Range Weather Forecasts (https://www.ecmwf.int/), and the CORDEX-Africa climatic data were obtained from the Earth System Grid Federation data node at the National Supercomputer Centre, Linköping, Sweden (https://esg-dn1.nsc.liu.se/projects/esgf-liu/). The authors acknowledge the World Climate Research Programme's Working Group on Regional Climate, and the Working Group on Coupled Modelling, former coordinating body of CORDEX and responsible panel for CMIP5, and all the modeling groups that produced and made available their model output. The population and urbanization data used in this research are available from their respective sources and the data produced within this study are available in Data Set S1.

References

Anderson, G. B., Bell, M. L., & Peng, R. D. (2013). Methods to calculate the heat index as an exposure metric in environmental health research. *Environmental Health Perspectives*, *121*(10), 1111–1119. https://doi.org/10.1289/ehp.1206273

Angel, S., Blei, A. M., Parent, J., Lamson-Hall, P., Galarza-Sanchez, N., Civco, D. L., et al. (2016). *Atlas of urban expansion—2016 Edition*. New York City, NY: NYU Urban Expansion Program and Lincoln Institute of Land Policy.

Angel, S., Parent, J., Civco, D. L., Blei, A., & Potere, D. (2011). The dimensions of global urban expansion: Estimates and projections for all countries, 2000–2050. *Progress in Planning*, *75*(2), 53–107. https://doi.org/10.1016/j.progress.2011.04.001

Asefi-Najafabady, S., Vandecar, K. L., Seimon, A., Lawrence, P., & Lawrence, D. (2018). Climate change, population, and poverty: Vulnerability and exposure to heat stress in countries bordering the Great Lakes of Africa. *Climatic Change*. https://doi.org/10.1007/s10584-018-2211-5

Bernhard, M. C., Kent, S. T., Sloan, M. E., Evans, M. B., McClure, L. A., & Gohlke, J. M. (2015). Measuring personal heat exposure in an urban and rural environment. *Environmental Research*, *137*, 410–418. https://doi.org/10.1016/j.envres.2014.11.002

Birkmann, J., Welle, T., Solecki, W., Lwasa, S., & Garschagen, M. (2016). Boost resilience of small and mid-sized cities. *Nature*, *537*, 605–608.

Bongaarts, J., & O'Neill, B. C. (2018). Global warming policy: Is population left out in the cold? *Science*, *361*(6403), 650–652. https://doi.org/10.1126/science.aat8680

Burkart, K., Khan, M. M., Schneider, A., Breitner, S., Langner, M., Kramer, A., & Endlicher, W. (2014). The effects of season and meteorology on human mortality in tropical climates: A systematic review. *Transactions of the Royal Society of Tropical Medicine and Hygiene*, *108*(7), 393–401. https://doi.org/10.1093/trstmh/tru055

CIESIN. (2011). Global Rural-Urban Mapping Project (GRUMP), version 1. Palisades, NY: NASA Socioeconomic Data and Applications Center (SEDAC). doi:https://doi.org/10.7927/H4GH9FVG

Coffel, E. D., Horton, R. M., & de Sherbinin, A. (2018). Temperature and humidity based projections of a rapid rise in global heat stress exposure during the 21st century. *Environmental Research Letters*, *13*(1), 014001. https://doi.org/10.1088/1748-9326/aaa00e

Crespo Cuaresma, J., Fengler, W., Kharas, H., Bekhtiar, K., Brottrager, M., & Hofer, M. (2018). Will the sustainable development goals be fulfilled? Assessing present and future global poverty. *Palgrave Communications*, *4*(1), 1–8. https://doi.org/10.1057/s41599-018-0083-y

Davis, R. E., McGregor, G. R., & Enfield, K. (2016). Humidity: A review and primer on atmospheric moisture and human health. *Environmental Research*, *144*, 106–116. https://doi.org/10.1016/j.envres.2015.10.014

Dee, D. P., Uppala, S. M., Simmons, A. J., Berrisford, P., Poli, P., Kobayashi, S., et al. (2011). The ERA-Interim reanalysis: Configuration and performance of the data assimilation system. *Quarterly Journal of the Royal Meteorological Society*, *137*(656), 553–597. https://doi.org/10.1002/qj.828

Donat, M. G., Alexander, L. V., Yang, H., Durre, I., Vose, R., Dunn, R. J. H., et al. (2013). Updated analyses of temperature and precipitation extreme indices since the beginning of the twentieth century: The HadEX2 dataset. *Journal of Geophysical Research: Atmospheres*, *118*, 2098–2118. https://doi.org/10.1002/jgrd.50150

Dong, W., Liu, Z., Liao, H., Tang, Q., & Li, X. (2015). New climate and socio-economic scenarios for assessing global human health challenges due to heat risk. *Climatic Change*, *130*(4), 505–518. https://doi.org/10.1007/s10584-015-1372-8

Dosio, A. (2016). Projections of climate change indices of temperature and precipitation from an ensemble of bias-adjusted high-resolution EURO-CORDEX regional climate models. *Journal of Geophysical Research: Atmospheres*, *121*, 5488–5511. https://doi.org/10.1002/2015JD024411

Dosio, A. (2017). Projection of temperature and heat waves for Africa with an ensemble of CORDEX Regional Climate Models. *Climate Dynamics*, *49*(1–2), 493–519. https://doi.org/10.1007/s00382-016-3355-5

Dosio, A., Mentaschi, L., Fischer, E. M., & Wyser, K. (2018). Extreme heat waves under 1.5°C and 2°C global warming. *Environmental Research Letters*, *13*(5), 054006. https://doi.org/10.1088/1748-9326/aab827

Filho, W. L., Balogun, A. L., Ayal, D. Y., Bethurem, E. M., Murambadoro, M., Mambo, J., et al. (2018). Strenghtening climate change adaptation capacity in Africa-case studies from six major African cities and policy implications. *Environmental Science and Policy*, *86*, 29–37. https://doi.org/10.1016/j.envsci.2018.05.004

GADM. (2018). Global administrative areas—version 3.6. Retrieved from https://gadm.org/data.html

Gao, J. (2017). Downscaling global spatial population projections from 1/8-degree to 1-km grid cells. NCAR Technical Note, NCAR/TN-537+STR. doi:https://doi.org/10.5065/D60Z721H

Gasparrini, A., Guo, Y., Hashizume, M., Kinney, P. L., Petkova, E. P., Lavigne, E., et al. (2015). Temporal variation in heat-mortality associations: A multicountry study. *Environmental Health Perspectives*, *123*(11), 1200–1207. https://doi.org/10.1289/ehp.1409070

Gasparrini, A., Guo, Y., Hashizume, M., Lavigne, E., Zanobetti, A., Schwartz, J., et al. (2015). Mortality risk attributable to high and low ambient temperature: A multicountry observational study. *The Lancet*, *386*(9991), 369–375. https://doi.org/10.1016/s0140-6736(14)62114-0

Gasparrini, A., Guo, Y., Sera, F., Vicedo-Cabrera, A. M., Huber, V., Tong, S., et al. (2017). Projections of temperature-related excess mortality under climate change scenarios. *The Lancet Planetary Health*, *1*(9), e360–e367. https://doi.org/10.1016/s2542-5196(17)30156-0

Georgescu, M., Morefield, P. E., Bierwagen, B. G., & Weaver, C. P. (2014). Urban adaptation can roll back warming of emerging megapolitan regions. *Proceedings of the National Academy of Sciences of the United States of America*, *111*(8), 2909–2914. https://doi.org/10.1073/pnas.1322280111

Guneralp, B., Zhou, Y., Urge-Vorsatz, D., Gupta, M., Yu, S., Patel, P. L., et al. (2017). Global scenarios of urban density and its impacts on building energy use through 2050. *Proceedings of the National Academy of Sciences of the United States of America*, *114*(34), 8945–8950. https://doi.org/10.1073/pnas.1606035114

Guo, Y., Gasparrini, A., Li, S., Sera, F., Vicedo-Cabrera, A. M., de Sousa Zanotti Stagliorio Coelho, M., et al. (2018). Quantifying excess deaths related to heatwaves under climate change scenarios: A multicountry time series modelling study. *PLoS Medicine*, *15*(7), e1002629. https://doi.org/10.1371/journal.pmed.1002629

Harrington, L. J., & Otto, F. E. L. (2018). Changing population dynamics and uneven temperature emergence combine to exacerbate regional exposure to heat extremes under 1.5 °C and 2 °C of warming. *Environmental Research Letters*, *13*(3), 034011. https://doi.org/10.1088/1748-9326/aaaa99

Hoornweg, D., & Pope, K. (2016). Population predictions for the world's largest cities in the 21st century. *Environment and Urbanization*, *29*, 195–246. https://doi.org/10.1177/0956247816663557

Houet, T., Marchadier, C., Bretagne, G., Moine, M. P., Aguejdad, R., Viguié, V., et al. (2016). Combining narratives and modelling approaches to simulate fine scale and long-term urban growth scenarios for climate adaptation. *Environmental Modelling & Software*, *86*, 1–13. https://doi.org/10.1016/j.envsoft.2016.09.010

IFPRI (2015). Urban extent of Africa 2010. International Food Policy Research Institute, Harvard Dataverse, version 1.5. doi:https://doi.org/10.7910/DVN/RUNZJD

IPCC (2012). *Managing the risks of extreme events and disasters to advance climate change adaptation: A special report of Working Groups I and II of the Intergovernmental Panel on Climate Change*. Cambridge, UK, and New-York City, NY: Cambridge University Press.

Jiang, L., & O'Neill, B. C. (2017). Global urbanization projections for the shared socioeconomic pathways. *Global Environmental Change*, *42*, 193–199. https://doi.org/10.1016/j.gloenvcha.2015.03.008

Jones, B., & O'Neill, B. C. (2016). Spatially explicit global population scenarios consistent with the shared socioeconomic pathways. *Environmental Research Letters*, *11*(8), 084003. https://doi.org/10.1088/1748-9326/11/8/084003

Jones, B., O'Neill, B. C., McDaniel, L., McGinnis, S., Mearns, L. O., & Tebaldi, C. (2015). Future population exposure to US heat extremes. *Nature Climate Change*, *5*(7), 652–655. https://doi.org/10.1038/nclimate2631

Jones, B., Tebaldi, C., O'Neill, B. C., Oleson, K., & Gao, J. (2018). Avoiding population exposure to heat-related extremes: Demographic change vs climate change. *Climatic Change*, *146*(3–4), 423–437. https://doi.org/10.1007/s10584-017-2133-7

KC, S., & Lutz, W. (2014). Demographic scenarios by age, sex and education corresponding to the SSP narratives. *Population and Environment*, *35*, 243–260. https://doi.org/10.1007/s11111-014-0205-4

KC, S., & Lutz, W. (2017). The human core of the shared socioeconomic pathways: Population scenarios by age, sex and level of education for all countries to 2100. *Global Environmental Change*, *42*, 181–192. https://doi.org/10.1016/j.gloenvcha.2014.06.004

Kriegler, E., O'Neill, B. C., Hallegatte, S., Kram, T., Lempert, R. J., Moss, R. H., & Wilbanks, T. (2012). The need for and use of socio-economic scenarios for climate change analysis: A new approach based on shared socio-economic pathways. *Global Environmental Change*, *22*(4), 807–822. https://doi.org/10.1016/j.gloenvcha.2012.05.005

Kuras, E. R., Richardson, M. B., Calkins, M. M., Ebi, K. L., Hess, J. J., Kintziger, K. W., et al. (2017). Opportunities and challenges for personal heat exposure research. *Environmental Health Perspectives*, *125*(8), 085001. https://doi.org/10.1289/EHP556

Kurniawan, R., & Managi, S. (2018). Measuring long-term sustainability with shared socioeconomic pathways using an inclusive wealth framework. *Sustainable Development*. https://doi.org/10.1002/sd.1722

Lemonsu, A., Viguié, V., Daniel, M., & Masson, V. (2015). Vulnerability to heat waves: Impact of urban expansion scenarios on urban heat island and heat stress in Paris (France). *Urban Climate*, *14*(4), 586–605. https://doi.org/10.1016/j.uclim.2015.10.007

Li, M., Gu, S., Bi, P., Yang, J., & Liu, Q. (2015). Heat waves and morbidity: current knowledge and further direction-a comprehensive literature review. *International Journal of Environmental Research and Public Health*, *12*(5), 5256–5283. https://doi.org/10.3390/ijerph120505256

Li, X., Zhou, Y., Eom, J., Yu, S., & Asrar, G. R. (2019). Projecting global urban area growth through 2100 based on historical time-series data and future Shared Socioeconomic Pathways. *Earth's Future*. https://doi.org/10.1029/2019EF001152

Liu, Z., Anderson, B., Yan, K., Dong, W., Liao, H., & Shi, P. (2017). Global and regional changes in exposure to extreme heat and the relative contributions of climate and population change. *Scientific Reports*, *7*, 43909. https://doi.org/10.1038/srep43909

Lwasa, S., Buyana, K., Kasaija, P., & Mutyaba, J. (2018). Scenarios for adaptation and mitigation in urban Africa under 1.5 °C global warming. *Current Opinion in Environmental Sustainability*, *30*, 52–58. https://doi.org/10.1016/j.cosust.2018.02.012

Matthews, T. K. R., Wilby, R. L., & Murphy, C. (2017). Communicating the deadly consequences of global warming for human heat stress. *Proceedings of the National Academy of Sciences of the United States of America*, *114*(15), 3861–3866. https://doi.org/10.1073/pnas.1617526114

Mishra, V., Mukherjee, S., Kumar, R., & Stone, D. (2017). Heat wave exposure in India in current, 1.5°C, and 2.0°C worlds. *Environmental Research Letters*, *12*, 124012. https://doi.org/10.1088/1748-9326/aa9388

Mora, C., Dousset, B., Caldwell, I. R., Powell, F. E., Geronimo, R. C., Bielecki, C. R., et al. (2017). Global risk of deadly heat. *Nature Climate Change*, *7*(7), 501–506. https://doi.org/10.1038/nclimate3322

NWS (2014). The heat equation index—Technical note. National Weather Service - Weather Prediction Center. Retrieved from. https://www.wpc.ncep.noaa.gov/html/heatindex_equation.shtml

OECD (2016). *African economic outlook 2016: Sustainable cities and structure transformation*. Paris: OECD Publishing. https://doi.org/10.1787/aeo-2016-en

O'Neill, B. C., Kriegler, E., Ebi, K. L., Kemp-Benedict, E., Riahi, K., Rothman, D. S., et al. (2017). The roads ahead: Narratives for shared socioeconomic pathways describing world futures in the 21st century. *Global Environmental Change*, *42*, 169–180. https://doi.org/10.1016/j.gloenvcha.2015.01.004

Papalexiou, S. M., AghaKouchak, A., Trenberth, K. E., & Foufoula-Georgiou, E. (2018). Global, regional, and megacity trends in the highest temperature of the year: Diagnostics and evidence for accelerating trends. *Earth's Future*, *6*, 71–79. https://doi.org/10.1002/2017ef000709

Pelling, M., Leck, H., Pasquini, L., Ajibade, I., Osuteye, E., Parnell, S., et al. (2018). Africa's urban adaptation transition under a 1.5° climate. *Current Opinion in Environmental Sustainability*, *31*, 10–15. https://doi.org/10.1016/j.cosust.2017.11.005

Rohat, G. (2018). Projecting drivers of human vulnerability under the shared socioeconomic pathways. *International Journal of Environmental Research and Public Health*, *15*(3). https://doi.org/10.3390/ijerph15030554

Rohat, G., Flacke, J., Dosio, A., Pedde, S., Dao, H., & van Maarseveen, M. (2019). Influence of changes in socioeconomic and climatic conditions on future heat-related health challenges in Europe. *Global and Planetary Change*, *172*, 45–59. https://doi.org/10.1016/j.gloplacha.2018.09.013

Russo, S., Marchese, A. F., Sillmann, J., & Immé, G. (2016). When will unusual heat waves become normal in a warming Africa? *Environmental Research Letters*, *11*(5), 054016. https://doi.org/10.1088/1748-9326/11/5/054016

Russo, S., Sillmann, J., & Sterl, A. (2017). Humid heat waves at different warming levels. *Scientific Reports*, *7*(1), 7477. https://doi.org/10.1038/s41598-017-07536-7

Satterthwaite, D. (2017a). Will Africa have most of the world's largest cities in 2100? *Environment and Urbanization*, *9*, 217–220. https://doi.org/10.1177/0956247816684711

Satterthwaite, D. (2017b). The impact of urban development on risk in sub-Saharan Africa's cities with a focus on small and intermediate urban centres. *International Journal of Disaster Risk Reduction*, *26*, 16–23. https://doi.org/10.1016/j.ijdrr.2017.09.025

Seto, K. C., Guneralp, B., & Hutyra, L. R. (2012). Global forecasts of urban expansion to 2030 and direct impacts on biodiversity and carbon pools. *Proceedings of the National Academy of Sciences of the United States of America*, *109*(40), 16,083–16,088. https://doi.org/10.1073/pnas.1211658109

Sheridan, S. C., & Allen, M. J. (2018). Temporal trends in human vulnerability to excessive heat. *Environmental Research Letters*, *13*(4), 043001. https://doi.org/10.1088/1748-9326/aab214

Sheridan, S. C., Allen, M. J., Lee, C. C., & Kalkstein, L. S. (2012). Future heat vulnerability in California, Part II: Projecting future heat-related mortality. *Climatic Change*, *155*(2), 311–326. https://doi.org/10.1007/s10584-012-0437-1

Sylla, M. B., Faye, A., Giorgi, F., Diedhiou, A., & Kunstmann, H. (2018). Projected heat stress under 1.5°C and 2°C global warming scenarios creates unprecedented discomfort for humans in West Africa. *Earth's Future*. https://doi.org/10.1029/2018ef000873

UN-Habitat (2015). Towards an Africa urban agenda. United Nations Human Settlements Programme and United Nations Economic Commission for Africa.

United Nations (2014). *World urbanization prospects: The 2014 revision*. New York: United Nations Department of Economics and Social Affairs, Population Division.

United Nations (2016). *Policies on spatial distribution and urbanization: Data booklet*. New York: United Nations Department of Economics and Social Affairs, Population Division. https://doi.org/10.18356/acb2c4c9-en

United Nations (2018). *World urbanization prospects: The 2018 revision*. New York: United Nations Department of Economics and Social Affairs, Population Division.

van Vuuren, D. P., Edmonds, J., Kainuma, M., Riahi, K., Thomson, A., Hibbard, K., et al. (2011). The representative concentration pathways: an overview. *Climatic Change*, *109*(1–2), 5–31. https://doi.org/10.1007/s10584-011-0148-z

Weber, T., Haensler, A., Rechid, D., Pfeifer, S., Eggert, B., & Jacob, D. (2018). Analyzing regional climate change in Africa in a 1.5, 2., and 3° global warming world. *Earth's Future*, *6*(4), 643–655. https://doi.org/10.1002/2017EF000714

Wisner, B., Pelling, M., Mascarenhas, A., Holloway, A., Ndong, B., Faye, P., et al. (2015). Small cities and towns in Africa: Insights into adaptation challenges and potentials. In S. Pauleit, G. Jorgensen, S. Kabisch, P. Gasparini, S. Fohlmeister, I. Simonis, K. Yeshitela, A. Coly, S. Lindley, & W. J. Kombe (Eds.), *Urban vulnerability and climate change in Africa* (pp. 153–196). New York: Springer.

Witmer, F. D. W., Linke, A. M., O'Loughlin, J., Gettelman, A., & Laing, A. (2017). Subnational violent conflict forecasts for sub-Saharan Africa, 2015-65, using climate-sensitive models. *Journal of Peace Research*, *54*(2), 175–192.

Zhao, L., Oppenheimer, M., Zhu, Q., Baldwin, J. W., Ebi, K. L., Bou-Zeid, E., et al. (2018). Interactions between urban heat islands and heat waves. *Environmental Research Letters*, *13*(3), 034003. https://doi.org/10.1088/1748-9326/aa9f73